Signatures of light-beam spatial filtering in a three-dimensional photonic crystal

L. Maigyte,[1] T. Gertus,[2,3] M. Peckus,[2] J. Trull,[1] C. Cojocaru,[1] V. Sirutkaitis,[2] and K. Staliunas[1,4]
[1]*Departament de Física i Enginyeria Nuclear, Universitat Politècnica de Catalunya, Colom 11, E-08222 Terrassa, Spain*
[2]*Laser Research Center, Vilnius University, Sauletekio al 10, LT-10222 Vilnius, Lithuania*
[3]*Altechna Co. Ltd., Konstitucijos 23 C, LT-08105 Vilnius, Lithuania*
[4]*Institució Catalana de Reserca i Estudis Avançats (ICREA), Pg. Lluis Companys 23, E-08010 Barcelona, Spain*
(Received 21 June 2010; published 13 October 2010)

We report experimental evidence of spatial filtering of light beams by three-dimensional, low-refraction-index-contrast photonic crystals. The photonic crystals were fabricated in a glass bulk, where the refraction index has been periodically modulated using tightly focused femtosecond laser pulses. We observe filtered areas in the angular distributions of the transmitted radiation, and we interpret the observations by theoretical and numerical study of light propagation in index-modulated material in paraxial model.

DOI: 10.1103/PhysRevA.82.043819 PACS number(s): 42.70.Qs, 42.55.Tv, 42.25.Fx, 42.79.−e

I. INTRODUCTION

Spatial filtering is broadly used to improve spatial quality of light beams [1]. The conventional technique of spatial filtering uses a confocal system of lenses to form the far-field image of the beam in the focal plane and a diaphragm of appropriate diameter to block the undesired large angle components of the spatial spectrum [2]. In the present article another, alternative, method for spatial filtering is experimentally demonstrated and theoretically analyzed. The method is based on the propagation of the beam through a specially designed photonic crystal (PC), where the undesired spatial spectra components are deflected to the first diffraction maxima of the periodic structure, whereas the "useful" part of the beam (corresponding to the central part of the spatial spectrum) remains in the central diffraction maximum and propagates in (and behind) the crystal without deflection.

The PCs, i.e., the materials with periodically spatially modulated refraction index on a wavelength scale, are widely studied mostly due to their peculiar *temporal* dispersion properties, in particular due to the appearance of the band gaps in *frequency* domain (see e.g., Refs. [3,4] for the photonic band gaps). Temporal dispersion is the frequency dependence of the propagation eigenmodes (Bloch modes) on the modulus of propagation wave number $\omega = \omega(|\vec{k}|)$. More recently it has been pointed out that the diffraction (the analog of *spatial* dispersion, i.e., the dependence of the longitudinal component of the propagation wavevector on its transverse component, $k_{||}(k_{\perp})$) can be also modified in PCs, managing the spatial propagation properties of the monochromatic light beams. The spatial propagation phenomena are usually interpreted in terms of isofrequency lines of the Bloch modes in (and behind) $\vec{k}$ space, i.e., $\omega(\vec{k}) = \text{const.}$, which indeed are the spatial dispersion (or diffraction) curves $k_{||}(k_{\perp})$. Whereas in isotropic materials the isofrequency lines are concentric circles, in PCs these circles become distorted due to the periodic modulation of the refraction index, leading to nontrivial spatial propagation effects. Perhaps the best-known propagation effect in PCs is the so-called self-collimation or the disappearance of diffraction [5–10], where, due to the flattening of the segments of the spatial dispersion curve the spatial envelope of the Bloch mode propagates without diffractive broadening. The dispersion curve can also present strongly tilted segments, which leads to super-refraction and negative refraction effects [11,12]. It has been recently proposed that the PCs can lead to the modification of the angular spectra of the transmitted beams [13], the effect that could be at the basis of an interesting type of spatial filter. Here we present the experimental signatures of the proposed filtering effect and give theoretical-numerical interpretation of the observations.

The mechanism of spatial filtering in PCs is more evident in the case when the propagation eigenmodes of the electromagnetic field display angular band gaps. Similarly to the band gaps in frequency domain $\omega(|\vec{k}|)$ which can be used to manipulate (to filter out) particular regions of the temporal spectrum [3,4], the angular band gaps could allow the manipulation of the angular or the spatial spectrum. Whereas the appearance of the frequency band gaps and the frequency filtering in one-dimensional (1D) PCs is related to the resonant back-scattering of the plane waves of particular frequencies, the spatial filtering is related with the resonant reflection or deflection of particular angular components of the light beam in 2D and 3D PCs, as illustrated in Figs. 1(a) and 1(b). The basic parameters of the PC, which determine the range of the wave components to be filtered out, are basically the longitudinal and transverse periods of the structure. In order to obtain an efficient spatial filter one aims to achieve high transparency for the axial and near-axial components, and low transparency (strong reflection or deflection) for particular angular (off-axis) components which are to be filtered out.

Here we consider another, less evident, mechanism of spatial filtering in PCs in the configuration displaying no angular band gaps. The idea of gapless filtering is that due to particular shapes of the spatial dispersion curve (in particular due to its strongly curved segments) the certain angular components of the beam can be deflected. Figure 1(b) illustrates the latter mechanism, which does not require the presence of the angular band gap. Differently from the first mechanism the angular components of the radiation do not reflect at the entrance of the PC, but instead deflect into the first diffraction maxima along the propagation in the PC.

As Fig. 1 highlights, the spatial filtering can be expected for the range of transverse component of the modulation wave vector $q_{\perp} \leqslant k$ (equivalently $d_{\perp} \geqslant \lambda$). The longitudinal period of the modulation determines whether the filtered

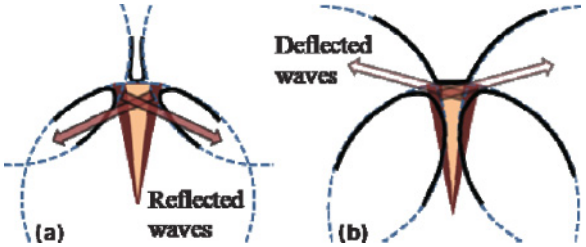

FIG. 1. (Color online) Illustration of the spatial filtering in a 2D PC in spatial Fourier plane (k_x, k_y) with (a) and without (b) the angular band gaps. Filtering occurs in both cases around the angles where the dispersion curves of the harmonic components for a particular frequency (dotted circles) cross. The spatial spectrum (far field) of the initial beam, consisting of the central (regular) part, and of the wings [the part to be removed, i.e., reflected in (a) or deflected in (b)], is illustrated with bright and dark triangles. The central dashed circle indicates the spatial dispersion of the homogeneous wave in homogeneous material, and the lateral circles indicate the dispersion of the lowest harmonic components in the PC.

angular components of the beam reflect in the backward direction ($2k > q_{||} > k$, equivalently $\lambda/2 < d_{||} < \lambda$) or deflect in the forward direction ($q_{||} < k$, equivalently $d_{||} > \lambda$). We considered the latter situation, as it corresponds to the PC used for the reported experiment on gapless filtering.

II. PHOTONIC CRYSTAL SAMPLES

Our PCs were fabricated by selectively modifying the refraction index of fused silica glass bulk by applying tightly focused femtosecond laser pulses [14–16]. The magnitude of the index change depends on material and exposition conditions. It is generally considered to be of the order of 10^{-3} [14–16]. The micromachining system used for fabrication operates with $\tau = 300$ fs duration pulses of $\lambda = 1030$ nm radiation with the energy of $E_{\text{imp}} = 1$ μJ and the repetition rate of $f = 200$ kHz. Glass samples were positioned using *XYZ* high-precision linear motor driven stages. The laser beam was focused using aspheric lens with $f = 4.03$ mm focal length and numerical aperture of 0.62, which resulted in a spot of ellipsoid shape at the focal point of width $w_\perp \approx 1$ μm and of length $w_{||} \approx 3$ μm.

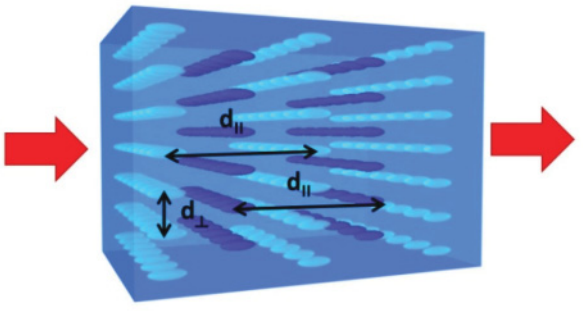

FIG. 2. (Color online) A side view of the PC. Ellipsoids indicate the areas illuminated by femtosecond pulses in the process of fabrication and correspond to the areas with enhanced refraction index in the PC.

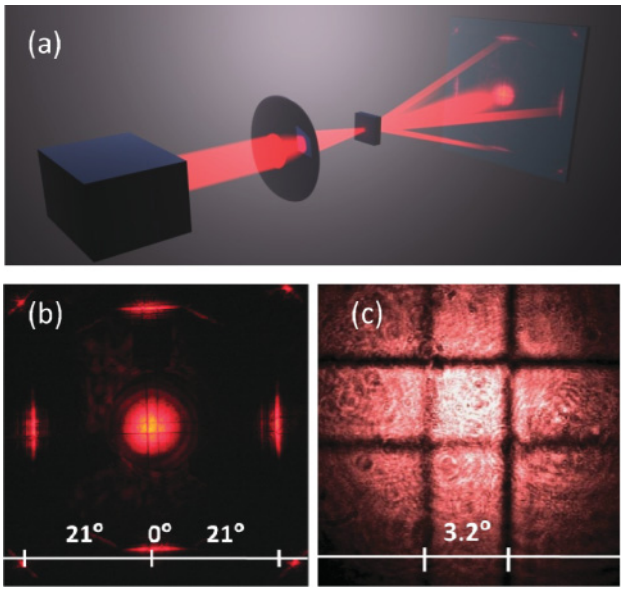

FIG. 3. (Color online) Experimental scheme (a) consisting of a focused laser beam (10× objective), PC sample at the focus, and a remote screen for observation of the far field. Results: (b) image on a screen indicating appearance of first-order diffraction maxima; (c) CCD camera image of the central part of the beam indicating angular field components filtered out (dark lines crossing each other and making a square in the central maximum).

The geometry of the PC is illustrated in Fig. 2, where $d_\perp = 1.5$ μm and $d_{||} = 10.6$ μm are the transverse and longitudinal periods, respectively. Different colors of the ellipsoids indicate odd and even layers of photonic crystal which are half-period shifted, one with respect to another in the transverse plane. The total number of the longitudinal modulation periods is 25 and the square structure in each transverse layer is 500 by 500 spots.

III. EXPERIMENTAL RESULTS

We illuminated the sample with a focused cw beam of a He-Ne laser of $\lambda = 633$ nm and the power up to 2 mW. The focused beam fits well inside the PC. The angular distribution of the intensity (distribution in the far-field domain) of the beam transmitted through the PC was observed on a screen and recorded by a charge-coupled device (CCD) camera. A schematic representation of the setup is presented in Fig. 3. The experimental measurement shows a clear presence of the first diffraction maxima [Figs. 3(a) and 3(b)] as well as the dark line structure in the central maximum [Figs. 3(b) and 3(c)].

The results are well reproducible (we used several PC samples fabricated under slightly different conditions) and show the signatures of the expected effect of the spatial filtering. The configuration of the crossing dark lines shows the filtered out angular components of the spatial spectra. The structure of these dark lines within the central maximum corresponds well to the structure of the bright lines observed in the first diffraction maxima, which is in good correspondence with the theoretical expectations discussed below.

Figure 4 represents a quantitative analysis of the spatial filtering effect. From the evaluation of the field distributions

follows that approximately 5% of the radiation energy was selectively removed from the central maximum and deflected into the four first order diffraction components. The angular intensity distribution of the deflected radiation coincides well with the angular distribution of the "dips" in the central components, as the comparison in Fig. 4 indicates.

IV. THEORY

We consider light propagation in a material with a spatially modulated refraction index, as described by paraxial model:

$$\left(2ik_0\,\partial/\partial z + \nabla_\perp^2 + 2\Delta n(x,y,z)k_0^2\right)A(x,y,z) = 0. \qquad (1)$$

Here $A(x,y,z)$ is the slowly varying complex envelope of the electromagnetic field in 3D space $E(x,y,z,t) = A(x,y,z)e^{ik_0z-i\omega_0t} + \text{c.c.}$ propagating along the z direction with the carrier wave number $k_0 = n\omega_0/c$ (in a material with average refraction index n) and $\nabla_\perp^2 = \partial^2/\partial x^2 + \partial^2/\partial y^2$ is the Laplace operator in the space transverse to the propagation direction.

The fabricated profile of the refraction index is well approximated by a harmonic function: $\Delta n(x,y,z) = \Delta n_0/4[\cos(q_x x) + \cos(q_y y)]\cos(q_z z)$, where Δn_0 is the maximum amplitude of the variation of the refractive index. We expand the field into harmonic components:

$$A(r_\perp,z) = \int e^{ik_\perp r_\perp}\left(A_0(k_\perp,z) + \sum_{m_x,m_y} A_{m_x,m_y}(k_\perp,z)e^{im_xq_xx+im_yq_yy-iq_zz}\right)dk_\perp \qquad (2)$$

containing only the most relevant diffracted components $A_{m_x,m_y}(k_\perp,z)\,[(m_x,m_y) = (0,-1),(0,+1),(-1,0),(+1,0)]$, in addition to the zero component $A_0(k_\perp,z)$. This particular truncation is justified having in mind the smallness of the index modulation, and also from the experimental observations, where only four diffraction maxima are dominating. $r_\perp = (x,y)$ denotes the space perpendicular to the propagation direction, and $k_\perp = (k_x,k_y)$ denotes the transverse components of the propagation wave vector. Inserting (2) into (1) results in the following:

$$\frac{d}{dz}A_0 = -\frac{ik_\perp^2}{2k_0}A_0 + \frac{i\Delta n_0k_0}{16}\sum_{m_x,m_y} A_{m_x,m_y}, \qquad (3a)$$

$$\frac{d}{dz}A_{m_x,m_y} = \left[-\frac{i(k_x+m_xq_x)^2 + i(k_y+m_yq_y)^2}{2k_0} + iq_z\right] \times A_{m_x,m_y} + \frac{i\Delta n_0k_0}{16}A_0, \qquad (3b)$$

where (3b) describes a coherent transport of the radiation from the central component $k_\perp = (k_x,k_y)$ to the diffracted components $(k_x + m_xq_x, k_y + m_yq_y)$, and (3a) describes a depletion of the zero component due to this scattering. The scattering and the depletion is most efficient for the angles $k_\perp$ corresponding to the resonant interaction between the zero component (3a) and one or several of the diffracted components (3b). The resonance condition reads:

$$(k_x + m_xq_x)^2 + (k_y + m_yq_y)^2 - 2q_zk_0 = k_x^2 + k_y^2 \qquad (4)$$

as follows from (3). This condition results in four crossing lines in $k_\perp$ space, each line corresponding to a particular set of (m_x,m_y), i.e., to the coupling with particular diffraction components. Physically speaking the radiation from each of the resonance lines is efficiently transported to their "own" diffraction components. The resonant lines are equivalent to the dark lines observed in experiment (Fig. 3). The pattern of the lines (the separation between the parallel lines) can be tuned by varying the parameters of the photonic structure. For instance all four lines cross at the center $k_x = k_y = 0$ for $q_x^2 = q_y^2 = 2k_0q_z$.

The resonance condition (4) allows calculating the angles of the dark lines with respect to the optical axis. In particular

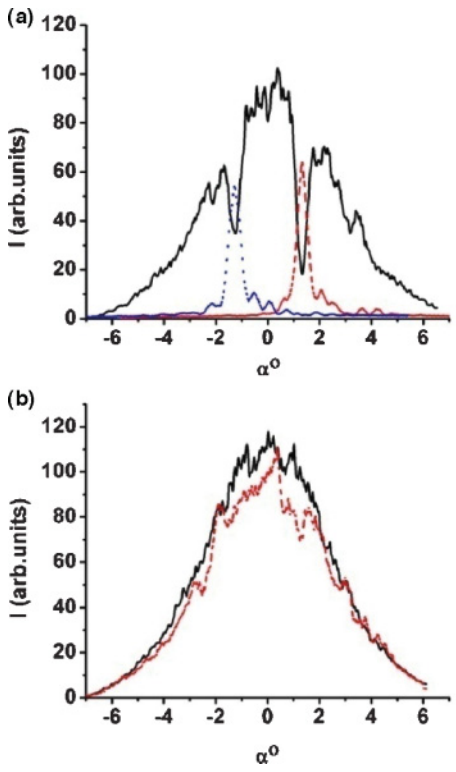

FIG. 4. (Color online) Intensity distributions well behind the PC (in the far-field domain) along the horizontal cut crossing the center of the beam: (a) the field from central maximum (solid line) and from the first diffraction maxima (dashed, colored lines). (b) Full transmitted intensity distribution, i.e., the central- and the first maxima added (dashed line) compared to the distribution without the crystal (solid line). α° is the angular coordinate (in degrees) in the far-field domain.

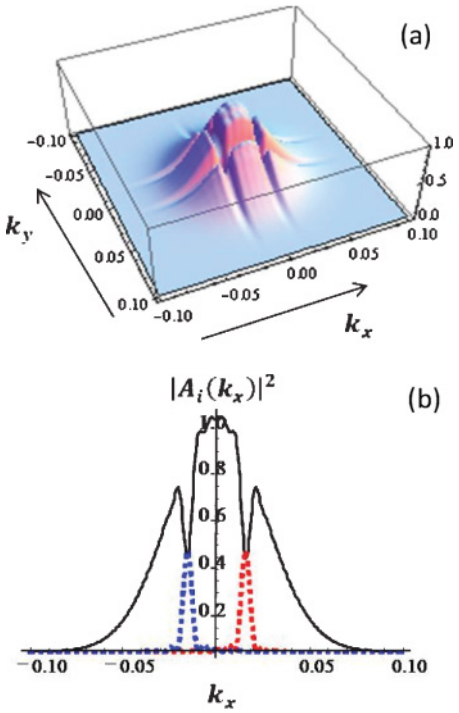

FIG. 5. (Color online) The 2D transmission profile (a) as well as the distribution on a horizontal cut (b), as obtained by numerical integration of (3) with the parameters: $f = 2 \times 10^{-4}$, $q_\perp = 0.25$, $q_{||} = 0.04$, and for normalized propagation distance $z = 4 \times 10^3$. The dimensional coupling factor: $fz = 0.8$.

the resonance line $(m_x,m_y) = (+1,0)$ appears at the position $k_x/k_0 = q_z/q_x - q_x/(2k_0)$ in the angular space. This latter expression was used to design the PCs with required resonance angle. In our samples the angle was engineered of 1.5°, as visible from Figs. 3(c) and 4(a).

The numerical integration of (3) shows the formation of the pattern in angular space (Fig. 5) which is analogous to that observed in experiment. The amplitude of the modulation of refraction index $\Delta n_0 = 3 \times 10^{-3}$ has been chosen in numerical calculations in order to match the experimental distributions from Fig. 4(a). In particular, the amplitude of the refraction index modulation in PC samples was estimated from the matching of experimental data with the theory and numerical results.

In order to explore the formation of a particular dark line we simplify the (3), by neglecting all the other resonances, except for a particular one (we consider the dark lines sufficiently separated). Considering the concrete resonance line $(m_x,m_y) = (+1,0)$ the evolution of the field components on the axis $k_y = 0$ follows:

$$\frac{d}{dz}A_0(k_x,z) = if A_{1,0}(k_x,z) \tag{5a}$$

$$\frac{d}{dz}A_{1,0}(k_x,z) = i\Delta k_z(k_x)A_{1,0}(k_x,z) + if A_0(k_x,z), \tag{5b}$$

where $\Delta k_z(k_x) = (2k_x q_x + q_x^2)/(2k_0) - q_z = \Delta k_x q_x/k_0$ is the off-resonance parameter for the interacting two waves (Δk_x is the transverse wave number with respect to the center of the dark line), and $f = \Delta n_0 k_0/16$ is the normalized parameter of coupling between the harmonic components (of dimension of inverse length).

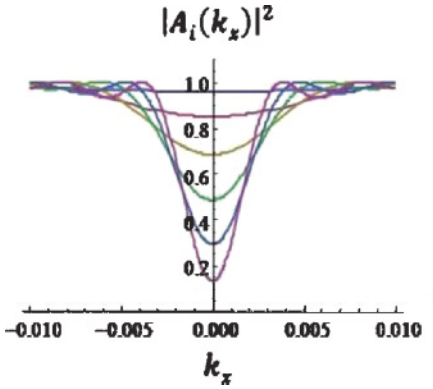

FIG. 6. (Color online) Evolution of the angular field profile around the resonance, as obtained from (6) along the propagation in PC. The parameters are $f = 2 \times 10^{-4}$, $q_\perp = 0.25$, $q_{||} = 0.04$, the lines show field profiles at equidistant propagation distances from $z = 0$ to $z = 6 \times 10^3$. (The adimensional coupling factor increases until $fz = 1.2$.)

The solution of (5a) is obtained analytically, which in terms of the field intensities reads:

$$|A_{1,0}(z)|^2 = \frac{|A_0(0)|^2 \sin^2\left(zf\sqrt{1 + \Delta k_z^2/(4f^2)}\right)}{1 + \Delta k_z^2/(4f^2)}(a) \tag{6a}$$

$$|A_0(z)|^2 = |A_0(0)|^2 - |A_{1,0}(z)|^2(b). \tag{6b}$$

The evolution of the far-field profile $|A_0(k_x,z)|^2$ along the propagation distance z is shown in Fig. 6. The dip in the central component increases, starts narrowing, and becomes maximally narrow at the full depletion. With increasing depth of the dip the oscillations on its fronts emerge. In particular the field components at the resonance $\Delta k_z = 0$ (i.e., on the center of the dark line) evolves with the propagation as $|A_0(z)|^2 = |A_0(0)|^2 \cos^2(fz) \approx |A_0(0)|^2(1 - f^2z^2/2)$. The half-width of the dark line decreases approximately as $\Delta k_{z,1/2}^2 \approx 2(3 - f^2z^2)/z^2$ (at the level of $\frac{1}{2}$ of intensity) as obtained by the series expansion of (6). The minimum half-width of the dark line at a distance of full depletion is $\Delta k_{z,1/2,\,\mathrm{min}} \approx f$. In terms of the variables of k_x, the half-width of the dark line evolves as $\Delta k_{x,1/2}^2 \approx 2k_0^2(3 - f^2z^2)/(q_x^2z^2)$ down to the minimum width of $\Delta k_{x,1/2,\,\mathrm{min}} \approx fk_0/q_x$.

The above derivations allow a simple estimation of the magnitude of the effect of spatial filtering for a given geometry of the PC: the minimum width of the dark line (in k space) is linearly proportional to the depth of index modulation and is given by $f = \Delta n_0 k_0/16$; the depth of the dark line is proportional to the adimensional coupling factor $fz = \Delta n_0 k_0 z/16$.

V. CONCLUSIONS

In conclusion, we have experimentally proved the effect of the spatial filtering of light beams by three-dimensional photonic crystals. Those evidences consist in the modification of the angular spectra of the propagating beams in such a way that the particular angular components are removed from the central diffraction maximum and are selectively deflected into

the first order diffraction maxima. Our theoretical-numerical analysis reproduces well the experimental observations and interprets the observed effect as the spatial filtering in the gapless configuration.

The reported effect of spatial filtering is relatively weak and carries a demonstrational character only, as the dark lines are relatively narrow. Only approximately 5% of the radiation was filtered out from the beam by the particular PC samples. The reason for the weak filtering is the relatively small amplitude of the modulation of the refraction index, resulting in weak coupling between the harmonic components. In order to obtain a technologically utile spatial filter the higher- (but moderate) index-contrast PCs are necessary, which are to be based on novel materials and new fabrication technologies. A technologically relevant spatial filtering, say, that allows improvement of the beam quality parameter by a factor of 2, requires selective removal of at least of 50% of the radiation. In this case the index modulation of order of $\Delta n_0 = 3 \times 10^{-2}$ would be needed for the same geometry and for the same width of the PC, as follows from the scaling of the strength of the effect derived above.

We note that the high-index-contrast PCs are not ideal for spatial filtering, as splitting of the dark lines according to theoretical predictions (6) occurs. This is, from an experimental viewpoint, should lead to a strong and unpredictable scattering of light by the PC structure. In this way the straightforward implementation of the high-index-contrast polymeric PCs, such as woodpiles [17,18] or fcc-like PC structure [19], could be problematic. However, the above-mentioned polymeric structures [17–19] filled by the material with the refraction index similar to that of a polymer, could lead to the desired refraction index contrast $\Delta n_0 = 3 \times 10^{-2}$ and could thus result in the above-estimated technologically spatial filtering effect (improving the beam quality parameter by the factor of two).

Finally, we highlight the advantages of the novel method of filtering presented in the present article. The main advantages (comparing with the conventional pinhole spatial filter) are as follows: (i) extremely small thickness (tenths or hundreds of microns) of the filter enabling the integration of such a filter into micro-optical devices or into microresonators of small lasers; (ii) translational invariance of the photonic crystal spatial filter (insensitivity to the lateral shift of PC structure) simplifying its utilization; and (iii) the possibility of combining (to add) the filtering functionality to some other, already existing, functionalities (amplification, nonlinearities) in bulk material by additional modulation of refraction index of the (amplifying or nonlinear) material.

ACKNOWLEDGMENTS

The work is financially supported by Spanish Ministerio de Educación y Ciencia and European FEDER through project FIS2008–06024-C03–02, the EC Seventh Framework Programme LASERLAB –EUROPE (Grant No. 228334), and by COST Action MP0702.

[1] A. E. Siegman, Proc. SPIE **1868**, 2 (1993).
[2] P. Hariharan, *Optical Holography* (Cambridge University Press, Cambridge, UK, 1996), pp. 74–75.
[3] E. Yablonovitch, Phys. Rev. Lett. **58**, 2059 (1987).
[4] S. John, Phys. Rev. Lett. **58**, 2486 (1987).
[5] H. Kosaka, T. Kawashima, A. Tomita, M. Notomi, T. Tamamura, T. Sato, and S. Kawakami, Appl. Phys. Lett. **74**, 1212 (1999).
[6] D. N. Chigrin, S. Enoch, C. S. Torres, and G. Tayeb, Opt. Express **11**, 1203 (2003).
[7] R. Illiew, C. Etrich, U. Peschel, F. Lederer, M. Augustin, H.-J. Fuchs, D. Schelle, E.-B. Kley, S. Nolte, and A. Tünnermann, Appl. Phys. Lett. **85**, 5854 (2004).
[8] D. W. Prather, S. Shi, D. M. Pustai, C. Chen, S. Venkataraman, A. Sharkawy, G. J. Schneider, and J. Murakowski, Opt. Lett. **29**, 50 (2004).
[9] K. Staliunas and R. Herrero, Phys. Rev. E **73**, 016601 (2006).
[10] Yu. Loiko, C. Serrata, R. Herrerob, and K. Staliunas Opt. Commun. **269**, 128 (2007).
[11] A. Lupu *et al.*, Opt. Express **14**, 2003 (2006).
[12] J. J. Baumberg, N. M. B. Perney, M. C. Netti, M. D. C. Charlton, M. Zoorob, and G. J. Parker, Appl. Phys. Lett. **85**, 354 (2004).
[13] K. Staliunas and V. J. Sánchez-Morcillo, Phys. Rev. A **79**, 053807 (2009).
[14] K. Kamata and M. Obara, Appl. Phys. A **78**, 85 (2004).
[15] R. R. Gattas and E. Mazur, Nat. Photonics **2**, 219 (2008).
[16] A. M. Streltsov and N. F. Borrelli, JOSA B **19**, 2496 (2002).
[17] M. Deubel, Georg von Freymann, Martin Wegener, Suresh Pereira, Kurt Busch, and Costas M. Soukoulis, Nat. Mater. **3**, 444 (2004).
[18] V. Mizeikis, K. K. Seet, S. Juodkazis, and H. Misawa, Opt. Lett. **29**, 2061 (2004).
[19] Jiaqi Chen, Wei Jiang, Xiaonan Chen, Li Wang, Sasa Zhang, and Ray T. Chen, Appl. Phys. Lett. **90**, 093102 (2007).